

Energy, Environmental, and Catalysis Applications

**Designing a novel polymer electrolyte for improving the electrode/electrolyte interface in flexible all-solid-state electrical double-layer capacitors**

Jeng-An Wang, Yi-Ting Lu, Sheng-Chi Lin, Yu-Sheng Wang, Chen-Chi Martin Ma, and Chi-Chang Hu

ACS Appl. Mater. Interfaces, Just Accepted Manuscript • DOI: 10.1021/acsami.8b02046 • Publication Date (Web): 10 May 2018

Downloaded from <http://pubs.acs.org> on May 14, 2018

**Just Accepted**

"Just Accepted" manuscripts have been peer-reviewed and accepted for publication. They are posted online prior to technical editing, formatting for publication and author proofing. The American Chemical Society provides "Just Accepted" as a service to the research community to expedite the dissemination of scientific material as soon as possible after acceptance. "Just Accepted" manuscripts appear in full in PDF format accompanied by an HTML abstract. "Just Accepted" manuscripts have been fully peer reviewed, but should not be considered the official version of record. They are citable by the Digital Object Identifier (DOI®). "Just Accepted" is an optional service offered to authors. Therefore, the "Just Accepted" Web site may not include all articles that will be published in the journal. After a manuscript is technically edited and formatted, it will be removed from the "Just Accepted" Web site and published as an ASAP article. Note that technical editing may introduce minor changes to the manuscript text and/or graphics which could affect content, and all legal disclaimers and ethical guidelines that apply to the journal pertain. ACS cannot be held responsible for errors or consequences arising from the use of information contained in these "Just Accepted" manuscripts.



ACS Publications

is published by the American Chemical Society, 1155 Sixteenth Street N.W., Washington, DC 20036

Published by American Chemical Society. Copyright © American Chemical Society. However, no copyright claim is made to original U.S. Government works, or works produced by employees of any Commonwealth realm Crown government in the course of their duties.

1  
2  
3  
4  
5  
6  
7  
8  
9  
10  
11  
12  
13  
14  
15  
16  
17  
18  
19  
20  
21  
22  
23  
24  
25  
26  
27  
28  
29  
30  
31  
32  
33  
34  
35  
36  
37  
38  
39  
40  
41  
42  
43  
44  
45  
46  
47  
48  
49  
50  
51  
52  
53  
54  
55  
56  
57  
58  
59  
60

# Designing a novel polymer electrolyte for improving the electrode/electrolyte interface in flexible all-solid-state electrical double-layer capacitors

Jeng-An Wang, Yi-Ting Lu, Sheng-Chi Lin, Yu-Sheng Wang, Chen-Chi M. Ma\* and Chi-Chang Hu\*

Department of Chemical Engineering National Tsing-Hua University Hsin-Chu 30013, Taiwan

## KEYWORDS

All-solid-state supercapacitor, gel polymer electrolyte, electrode/electrolyte interface, polyacrylic acid, waterborne polyurethane, crosslinking.

## ABSTRACT

A novel copolymer, polyurethane-polyacrylic acid, is successfully synthesized from polyacrylic acid (PAA) backbone cross-linked with waterborne polyurethane (WPU). This sticky polymer, which is neutralized with 1 M KOH and then soaked in 1 M KOH (denoted as WPU-PAAK-K), provides an ionic conductivity greater than  $10^{-2}$  S cm<sup>-1</sup> and acts as a gel electrolyte perfectly improving the electrode/electrolyte interfaces in a flexible all-solid-state electrical double-layer capacitor (EDLC). The PAA backbone chains in the copolymer increase the amount of carboxyl groups and promote the segmental motion. The carboxyl groups enhance the water-uptake capacity, which facilitates the ion transport and promotes the ionic conductivity. The cross-

linked agent, WPU chains, effectively maintains the rich water content and provides mechanical stickiness to bind two electrodes together. An acid-treated carbon paper (denoted as ACP) combining with such a gel polymer electrolyte demonstrates excellent capacitive behavior with a high areal capacitance of  $211.6 \text{ mF cm}^{-2}$  at  $10 \text{ mV s}^{-1}$ . A full cell consisting of ACP/WPU-PAAK-K/ACP displays a low equivalent series resistance of  $0.44 \Omega$  from the electrochemical impedance spectroscopic results. An all solid-state ACP/WPU-PAAK-K/ACP EDLC provides an areal specific capacitance of  $94.6 \text{ mF cm}^{-2}$  at  $1 \text{ mA cm}^{-2}$ . This device under  $180^\circ$  bending shows a capacitance retention over 90 %, revealing its remarkable flexibility.

## INTRODUCTION

Supercapacitors (SCs), one kind of energy storage devices, also known as electro-chemical capacitors or ultracapacitor,<sup>1-2</sup> have attracted considerable attention and aroused extensive research due to its superior cycle life, high power ability, short charging time, and excellent reliability in comparison with rechargeable batteries. A typical SC usually consists of a separator, two electrodes and a liquid electrolyte. However, due to the emerging demand of wearable devices, flexible SCs are widely investigated. Among flexible SCs, a lot of flexible materials, including polymer films,<sup>3-5</sup> carbon papers,<sup>6-7</sup> fibers,<sup>8-9</sup> and fabrics<sup>10-12</sup> have been applied to produce the flexible electrodes.

Besides electrode materials, the electrolyte plays an equally important role in the commercial application. Commonly, SCs employ liquid electrolytes because of highly ionic conductivity, inevitably resulting in the problems of leakage during the long-time usage/storage. Accordingly, replacing liquid electrolytes with solid/gel electrolytes enhances the safety and flexibility of SCs. Recently, several studies are devoted to solid-polymer or gel-polymer electrolytes, in order to

1  
2  
3 develop the all solid-state and quasi-solid-state SCs since these devices offer attractive features  
4 such as easy fabrication, no liquid leakage, long shelf life, and high safety.<sup>13-17</sup>  
5  
6

7  
8 In general, solid polymer electrolytes suffer from the disadvantage of low ionic conductivity,  
9 leading to a high equivalent series resistance (ESR). In contrast, gel polymer electrolytes (GPEs)  
10 provide numerous channels for ion transport within polymer matrix and high ionic conductivity,  
11 because the absorbed solvent enlarges the space between polymer chains, which are desirable for  
12 the high power SCs. Among the current ionic conducting gels, potassium polyacrylate (PAAK)  
13 is a promising GPE for electrochemical energy storage devices.<sup>18</sup> Compared with polyvinyl  
14 alcohol (PVA) and polyethylene oxide (PEO),<sup>18</sup> the polyacrylate backbone exhibits a higher  
15 ionic conductivity because of its higher segmental motion.<sup>18</sup> In addition, this polymer  
16 containing negatively charged carboxyl groups in the side chains exhibited additional cationic  
17 conductivity since the potassium ions can exchange among these groups.<sup>19</sup> From the literature,<sup>20</sup>  
18 a 7% PAAK polymer dispersed in the 6 M KOH solution provided a high ionic conductivity of  
19  $6 \times 10^{-1}$  S cm<sup>-1</sup>, meanwhile the carboxylate groups on the PAAK backbone have strong affinity  
20 toward the electrodes due to its high polarity, which increases the electrode/electrolyte interfacial  
21 area, leading to a good capacitive performance.  
22  
23

24 Polyurethane (PU) self-standing thin films have been reported to possess great mechanical  
25 strength, toughness and good ion conductivity of lithium ions because the polymer chain  
26 includes both soft and rigid segments.<sup>21-23</sup> The mobility of polymer chains can be tuned by  
27 altering the length and the type of soft segments (polyol) and rigid segments (isocyanate).  
28 Commercially, PUs are used to produce glues due to their sticky property, and PU glues work  
29 well on a variety of materials, whether they are porous or not, e.g., wood, metals, rubbers, cured  
30 epoxy, leather, tile and glass, many plastics, concrete, and brick. However, more than 90% PU  
31  
32

1  
2  
3 products contain organic solvents, including dimethylformamide (DMF), dimethylacetamide  
4 (DMAc), toluene, hexane, or 1-methyl-2-pyrrolidone (NMP). With the rise of environmental  
5 awareness, removal of organic solvents and synthesis of nontoxic PUs are in demand. Therefore,  
6 waterborne PUs (WPUs) become more and more important and have become one of the most  
7 popular products in the PU industry on account of their environmentally benign manufacture  
8 process.<sup>24</sup>

9  
10 Based on all the above considerations, we try to synthesize a novel cross-linked polymer which  
11 consists of PAAK and WPU. The WPU chain (with low  $T_g$  and  $T_m$ ) cross-linked with the PAAK  
12 backbone not only forms a tough network to soak liquid electrolytes but also keeps good  
13 flexibility in order to enhance its ionic conductivity. Furthermore, the intrinsic mobility of WPU  
14 chains can prevent the flexibility of GPEs from deteriorating, when the solvent molecules in the  
15 liquid electrolytes evaporate into the air. Consequently, the introduction of this sticky WPU-  
16 PAAK-K GPE can provide excellent adhesion to closely assemble two carbon paper electrodes  
17 without any package process and improve the electrode/electrolyte interface contact to enhance  
18 the capacitive performance of EDLCs.

19  
20  
21  
22  
23  
24  
25  
26  
27  
28  
29  
30  
31  
32  
33  
34  
35  
36  
37  
38  
39 EXPERIMENTAL SECTION

40  
41  
42 1. Materials

43  
44  
45 YA-7720 polyester polyol was purchased from Coating Chemical Industry Co., Taiwan.  
46 Hexamethylene diisocyanate (HDI) was from Tokyo Chemical Industry Co., Japan. Di-n-butyltin  
47 dilaurate (DBTDL) was from Alfa Aesar, Germany. 2,2-bis(hydroxymethyl)propionic acid  
48 (DMPA), acrylic acid, and acrylamide were purchased from Acros Organics Co., USA.  
49 Potassium persulfate (KPS), 1-ethyl-3-(3-dimethylaminopropyl)carbodiimide hydrochloride  
50  
51  
52  
53  
54  
55  
56  
57  
58  
59

(EDC), N-hydroxy-succinimide (NHS), potassium poly(acrylate) (PAAK), and polyvinyl alcohol (PVA) were from Sigma-Aldrich Chemie, Germany. The commercial carbon paper BC 24 was purchased from SGL Graphite Solutions Co., Germany.

## 2. Synthesis of WPU-PAA copolymer

Polyurethane was synthesized from a mixture of HDI, YA7720, and DMPA in the molar ratio of 1.6:1:0.6, dissolved in 50 g methyl ethyl ketone (MEK) and heated to 70°C. Then, the DBTDL catalyst was added to accelerate the reaction for 5 h. Next, deionized water was slowly added into the PU-MEK solution by a digital peristaltic pump. When the solution became homogeneously mixing, WPU, well dispersed in water, was formed from the removal of MEK by the rotary evaporation. Polyacrylic acid (PAA) was synthesized by the free radical polymerization from 15 g acrylic acid mixed with acrylamide and 0.1 wt% KPS initiator in 60-ml deionized water. To make the cross-linked structure, the carboxylic groups of WPU were activated (active carboxylic groups) by NHS/EDC catalysts. The formation of imide groups from the reaction between the active carboxylic groups on WPU and the amide groups on PAA formed the cross-linked structure. Finally, the WPU-PAA solution was titrated with 1 M KOH to form the potassium salts on the carboxylic groups (-COO<sup>-</sup>K<sup>+</sup>). After overnight drying in a vacuum oven at 80°C, WPU-PAAK particles were obtained.

## 3. Preparation of ACP electrode and GPE

Acid-treated carbon papers (ACPs) were prepared from commercial carbon papers (CPs) with an oxidation treatment.<sup>25</sup> Before the oxidation treatment, CP was cold-rolled in a stainless steel roller with a gap of 100 μm to enhance its flexibility. This CP rinsed with deionized water was immersed in a mixture of sulfuric acid and nitric acid in 3:1 weight ratio at 60°C for 2 h. Then, the CP was rinsed with deionized water and dried at 80°C in an oven for 8 h to obtain the ACP

1  
2  
3 with thickness about 80  $\mu\text{m}$ . The WPU-PAAK particles and commercial polymers (PAAK and  
4  
5 PVA) were soaked with 1 M KOH with the KOH solution-to-polymer mass ratio varying from  
6  
7 100 to 500% (denoted as soaking ratio), which were shaken at 200 rpm in a water bath at room  
8  
9 temperature overnight. Finally, the homogeneous WPU-PAAK-K, PVA-K and PAAK-K GPEs  
10  
11 were obtained.  
12  
13

14  
15 4. Assembly of ACP/GPE/ACP devices  
16  
17

18 The electrochemical performances were measured in a coin cell which was assembled with two  
19 ACP electrodes, a GPE film, and stainless steel (SS) current collectors (see the assembly scheme  
20 in Figure 1a). The circular ACP electrodes with a diameter of 2 cm were pasted onto the SS  
21 current collectors by the conductive carbon glue. Then, the GPE was tightly clamped by two  
22 electrodes to form the full cell. Note that an all solid-state cell without any package was also  
23 assembled to show the unique adhesive and bending characteristics of our GPE. For this cell, two  
24 ACP strips with a geometric area of  $1 \times 5$  cm were pasted onto the titanium foil of the same size  
25 to form bendable electrodes (Ti/ACP). Next, Ti/ACP, GPE, and ACP/Ti were closely stacked  
26 layer by layer with a cold pressing to form the all solid-state cell (see Figure 1b). For the above  
27 two devices, the thickness of GPE films was controlled to be  $2 \pm 0.1$  mm.  
28  
29  
30  
31  
32  
33  
34  
35  
36  
37  
38  
39  
40  
41  
42  
43  
44  
45  
46  
47  
48  
49  
50  
51  
52  
53  
54  
55  
56  
57  
58  
59  
60

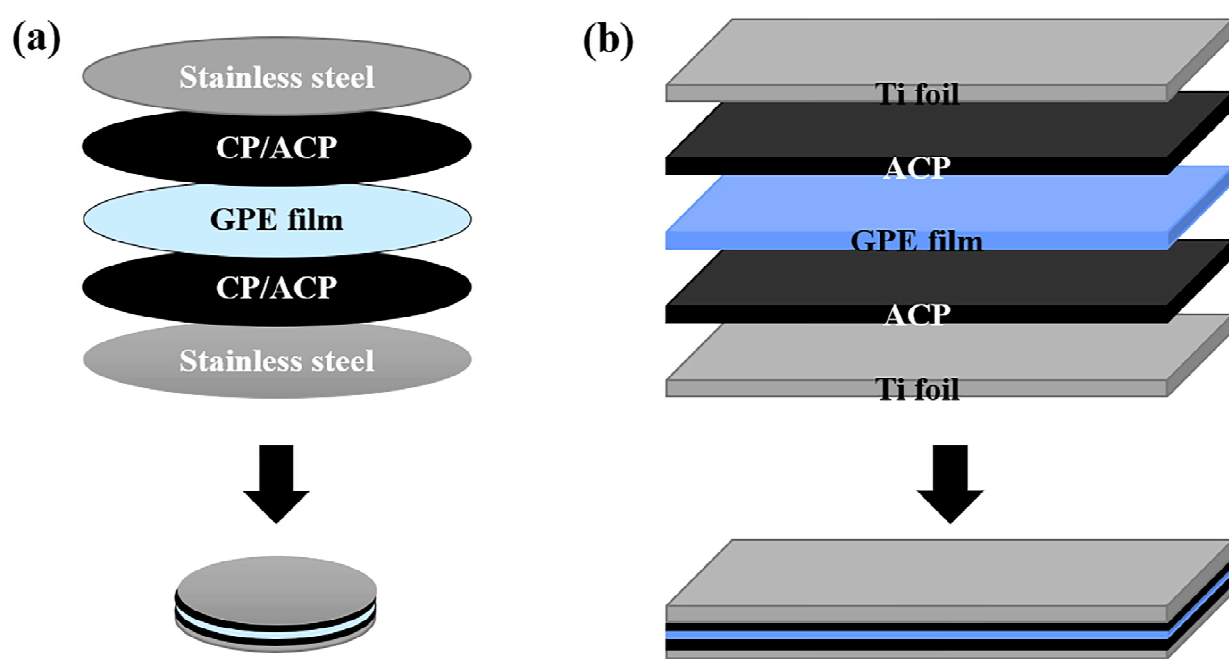


**Figure 1.** The assembly schemes of (a) a coin cell and (b) an all solid-state EDLC.

## 5. Characterization

The surface morphology of GPEs was examined by a Hitachi S-4700I field-emission scanning electron microscope (FE-SEM). The chemical environments of GPEs were obtained by a PHI Quantera X-ray photoelectron spectroscope (XPS) using an Al K $\alpha$  X-ray source. The water retention of GPEs could be estimated from the weight loss data according to equation (1):

$$\text{Water retention} = \frac{W - W_{\text{polymer}}}{W_{\text{total}} - W_{\text{polymer}}} \quad (1)$$

where  $W_{\text{polymer}}$  (in g) is the mass of dried GPEs,  $W_{\text{total}}$  is the initial total mass of GPEs soaked with 1 M KOH, and  $W$  is the mass of corresponding GPEs measured on different days. The adhesion property of GPEs was examined by the SEM cross section images and the 180° peel test which was analyzed by an AGS-2000G universal testing/tensile testing machine. For the 180° peel test, GPEs were coated on the titanium foil with a fixed contact area of 10 × 30 mm.

The next step is to use another titanium foil covering on it to form a sandwich structure for the tensile test.

All electrochemical tests were conducted by an electrochemical analyzer (CHI 6273E, CH Instruments, Inc., USA). The ionic conductivities ( $\sigma$ ) of GPEs were deduced from the electrochemical impedance spectroscopic (EIS) data according to equation (2) where L (cm) is thickness, R ( $\Omega$ ) is the resistance, and A ( $\text{cm}^2$ ) is the area of the GPE film.

$$\sigma = \frac{L}{RA} \quad (2)$$

The area-specific capacitance of a full cell for the all solid-state EDLC could be evaluated by the cyclic voltammograms (CVs) on the negative sweeps through equation (3) (i.e.,  $C_{fc-cv}$ ) or by the galvanostatic charge-discharge curve using equation (4). The area-specific capacitance of ACP ( $C_{s,ACP}$ ) was deduced from  $C_{fc-cv}$  or  $C_{fc-cp}$  (i.e.,  $1/C_{fc} = 1/C_{s,ACP}^+ + 1/C_{s,ACP}^-$ ).

$$C_{fc-cv} = \frac{1}{AvU} \int_0^V idU \quad (3)$$

$$C_{fc-cp} = \frac{it}{AU} \quad (4)$$

where  $v$  is the scan rate of CV,  $i$  is the voltammetric or charge-discharge current,  $t$  (s) is the discharge time, and U (V) is the cell voltage. The specific energy density was obtained from  $C_{fc-cp}$  according to equation (5):

$$E = \frac{1}{2 \times 3.6} C_{fc-cp} \cdot U^2 \quad (5)$$

The specific power density of this EDLC was deduced by equation (6):

$$P = \frac{3600E}{t} \quad (6)$$

## RESULTS AND DISCUSSION

### 1. Characterization of WPU-PAA copolymer

The cross-linked structure between WPU and PAA was designed by the formation of the imide groups from the reaction between the active carboxylic groups on WPU and the amide groups on PAA (see Figure 2(a)). To confirm the successful formation of imide groups between the polymer chains of WPU and PAA, XPS was used to analyze the chemical composition of PAA, WPU, and WPU-PAA. The C1s core level spectra of PAA, WPU and WPU-PAA are shown in Figures 2(b)-2(d), respectively. In Figure 2(b), the C1s peak can be deconvoluted into three main constituents corresponding to the typical bonding of PAA, i.e., C-C, C-C=O, and O-C=O.<sup>26</sup> The rich content of the C-C single bond indicates the successful radical polymerization of acrylic acids to form linear polymer chains. The C-C=O and O-C=O peaks come from the carboxylic groups on the side chains of PAA. In Figure 2(c), the C1s core level spectrum of WPU revealed the presence of C-C, C-O, C-N, C-C=O, and O-C=O structures.<sup>27</sup> The peak of the C-C single bond demonstrates a long alkyl backbone in WPU. In addition, there are a lot of ester groups and amide groups on the backbone coming from the soft segments (polyol YA7720) and hard segments (HDI), indicated by the C-O and C-N peaks, respectively. Besides polyol YA7720, DMPAs also provide the soft segments in the backbone. Their carboxylic groups on the side chains result in the signals of C-C=O and O-C=O. On the other hand, most of the O-C=O signal should be contributed by the ester groups in polyol YA7720. The C1s core level spectrum of WPU-PAA in Figure 2(d) also indicates the presence of five structures corresponding to C-C, C-C=O, C-N, C-O and O-C=O groups. Compared to WPU, an increase in the signals of C-C=O and O-C=O was expected because of the introduction of PAA. However, this phenomenon is not found for the O-C=O group, reasonably attributed to the formation of imide groups since the

reaction between activated carboxylic groups on WPU and amide groups on PAA reduces the content of the O-C=O bond. Furthermore, the ratio of C-N/C-O in WPU-PAA is obviously higher than that in WPU, reasonably due to the contribution from the imide groups. The above results suggest the formation of imide groups, demonstrating the successful formation of the cross-linked structure between WPU and PAA.

Figures 2(e) and 2(f) show the XPS N1s core level spectra to detail the chemical environment of nitrogen. In Figure 2(e), the N1s peak is only ascribed to the N-(C=O)-O bond ( $400.3 \pm 0.1$  eV)<sup>28</sup> which is the typical urethane functional group in WPU, confirming the successful synthesis of WPU. In Figure 2(f), an additional peak located at 400.6 eV indicates the formation of (C=O)-N-(C=O) bonds.<sup>28</sup> This nitrogen bonding structure is reasonably attributed to the formation of imide groups between WPU and PAA, consistent with the results of the C1s data.

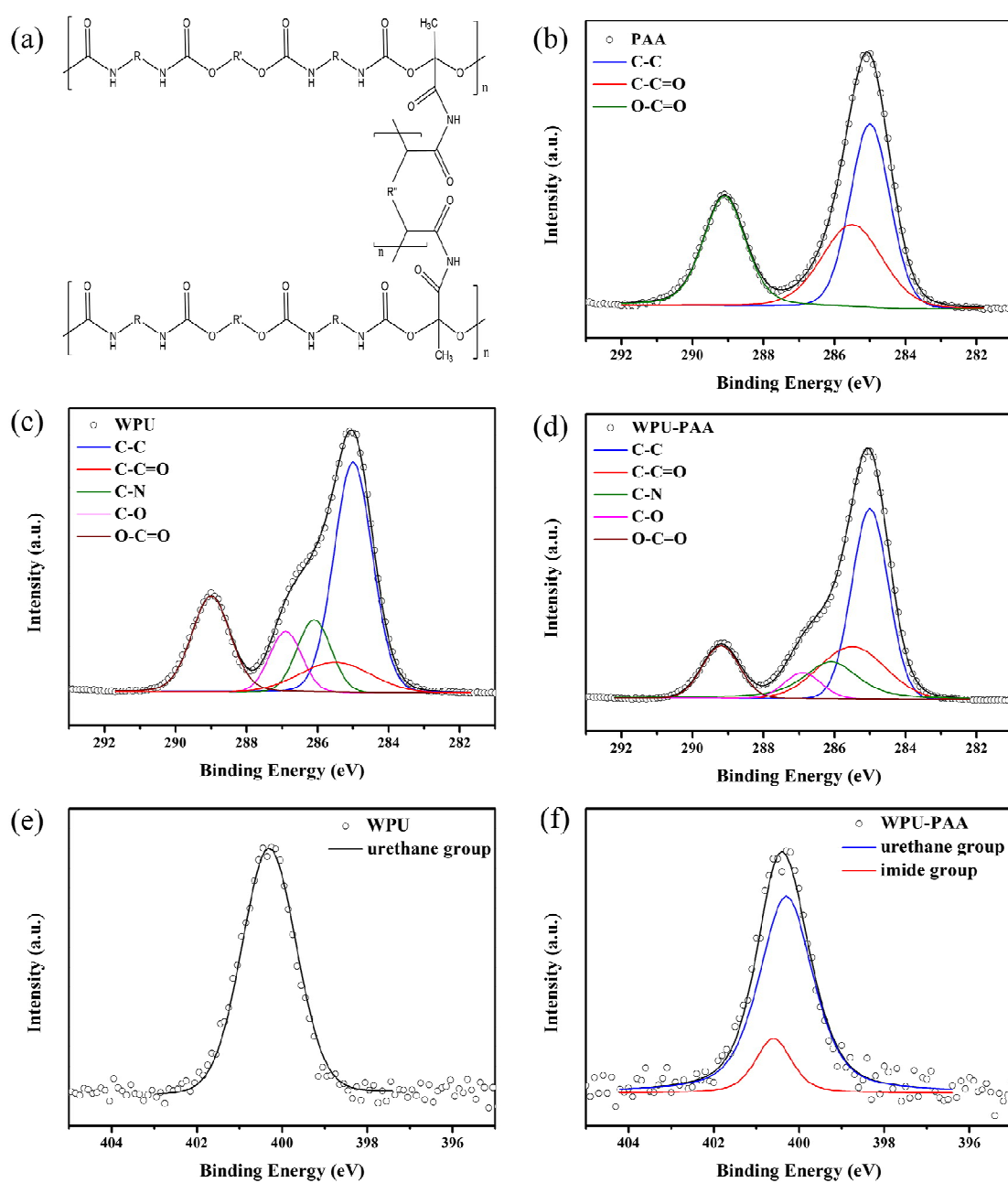


**Figure 2.** (a) The structure of WPU-PAA (R: HDI, R': polyol YA7720 and R'': PAA) and the XPS core-level spectra of (b-d) C1s and (e,f) N1s peaks for (b) PAA, (c,e) WPU, and (d,f) WPU-PAA.

1  
2  
3    2. Ionic conductivity of GPE-K  
4  
5  
6  
7  
8  
9  
10  
11  
12  
13  
14  
15

The ionic conductivities of GPE-K were deduced from the EIS spectra of a coin cell. The WPU-PAAK-K, PVA-K, and PAAK-K polymer hydrogels were the GPE films fitted between two stainless steel electrodes. Due to the requirement of high ionic conductivity on GPE films, the ionic conductivity of various GPE films in various soaking ratios was measured and typical results are shown in Figure 3.

From an examination of Figure 3(a), three features had to be discussed. First, for the cells using WPU-PAAK-K and PAAK-K, the ionic conductivity is almost as high as  $10^{-1}$  S cm $^{-1}$ , which is higher than  $10^{-2}$  S cm $^{-1}$  for the cell employing the PVA-K GPE. The relatively higher conductivities of WPU-PAAK-K and PAAK-K in comparison with that of PVA-K are attributable to the extra ionic conductivity from their carboxylic groups with cations. In addition, the WPU-PAAK film soaked with the KOH solution always exhibits the highest ionic conductivity at any specified soaking ratio owing to the high flexibility of this polymer. Note that the cross-linked structure can reduce the crystallization of linear polymers, favoring the ion transportation<sup>29</sup> and the soft WPU can avoid the formation of rigid polymer network, which maintains the facile segmental motion of polymer. Second, the ionic conductivity of each GPE becomes higher with increasing the soaking ratio, especially for the soaking ratios lower than 200%. This phenomenon is reasonably attributed to the formation of more ionic tunnels within GPE films with more electrolyte uptake.<sup>29-30</sup> In other words, when the soaking ratios are too low, the tangled polymer chains within the GPE films retard the segmental motion of polymer chains, resulting in a relatively high barrier for ion movement. When the soaking ratios become high enough, the polymer chains are disentangled in the alkaline solution and more ionic tunnels are formed to promote the ion transportation. However, the ionic conductivity of GPE is not

significantly enhanced by the more alkaline electrolyte uptake when the soaking ratios are higher than 200 %, probably due to the formation of continuous ion-conductive network by the complete dispersion of polymer chains. This phenomenon also suggests that the ion mobility within electrolyte-enriched GPEs is similar to the bulk electrolyte solutions. Third, when the soaking ratios are lower than/equal to 200%, the WPU-PAAK-K film shows a good mechanical property due to the significant content of tangled polymer chains in this GPE film. Again, the poor mechanical property of GPEs results from a too high water content making the polymer chains fully disperse. Accordingly, our WPU-PAAK-K film with the 200% soaking ratio is a desirable GPE because of its enough mechanical strength (see inset in Figure 3(a)) and high ionic conductivity.

In order to compare the moisture adsorption/desorption ability of GPEs from the ambient environment, all GPE films were exposed to the ambient air with the relative humidity fluctuated between 63 to 75 % for 2 weeks and their results of water retention and ionic conductivity are shown in Figures 3(b) and 3(c). From Figure 3(b), a gradual decrease in the water retention was observed for all GPE films during the first week. This phenomenon was attributable to the dry environment which gave rise to the desorption of water molecules during the first week. Then, the water retention reached a steady state after a week due to the balanced adsorption and desorption of the moisture. In comparison with the hydroxyl functional groups in PVA, the carboxyl functional groups in PAAK and WPU-PAAK exhibit higher polarity, leading to higher water retention ability. The cross-linked structure of WPU-PAAK further improves the water retention and consequently, the WPU-PAAK-K film could exhibit high ionic conductivity of  $3.2 \times 10^{-2}$  S cm<sup>-1</sup>, in exposure to the air for two weeks. This value is still higher than  $1.6 \times 10^{-2}$  and  $3 \times 10^{-3}$  S cm<sup>-1</sup> for the PAAK-K and PVA-K films, respectively. Moreover, with respect to

flexibility, the PVA-K and PAAK-K films become tough and lose their flexibility during this test because of a too high content of the tangled polymer chains. Owing to the high mobility of WPU chains, the WPU-PAAK-K film shows high flexibility after the above exposure in the air for two weeks (see Figure 3(d)).

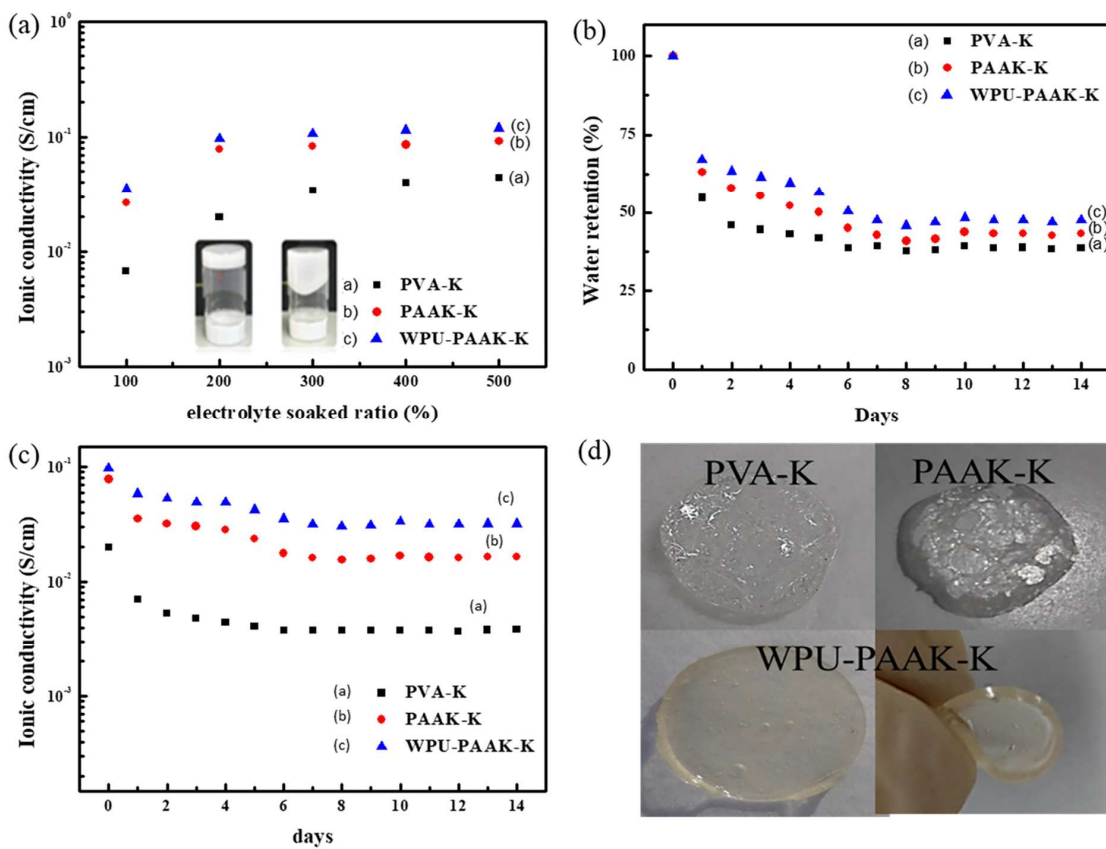


**Figure 3.** (a) Ionic conductivity of various polymers against the soaking ratio of 1 M KOH electrolyte; inset shows the photographs of WPU-PAAK with the soaking ratios equal to 200 and 300%. (b) The water retention and (c) ionic conductivity of GPE films with the 200 % soaking ratio against the exposure time in air for 2 weeks. (d) Photographs of GPE films after exposure in air for 2 weeks.

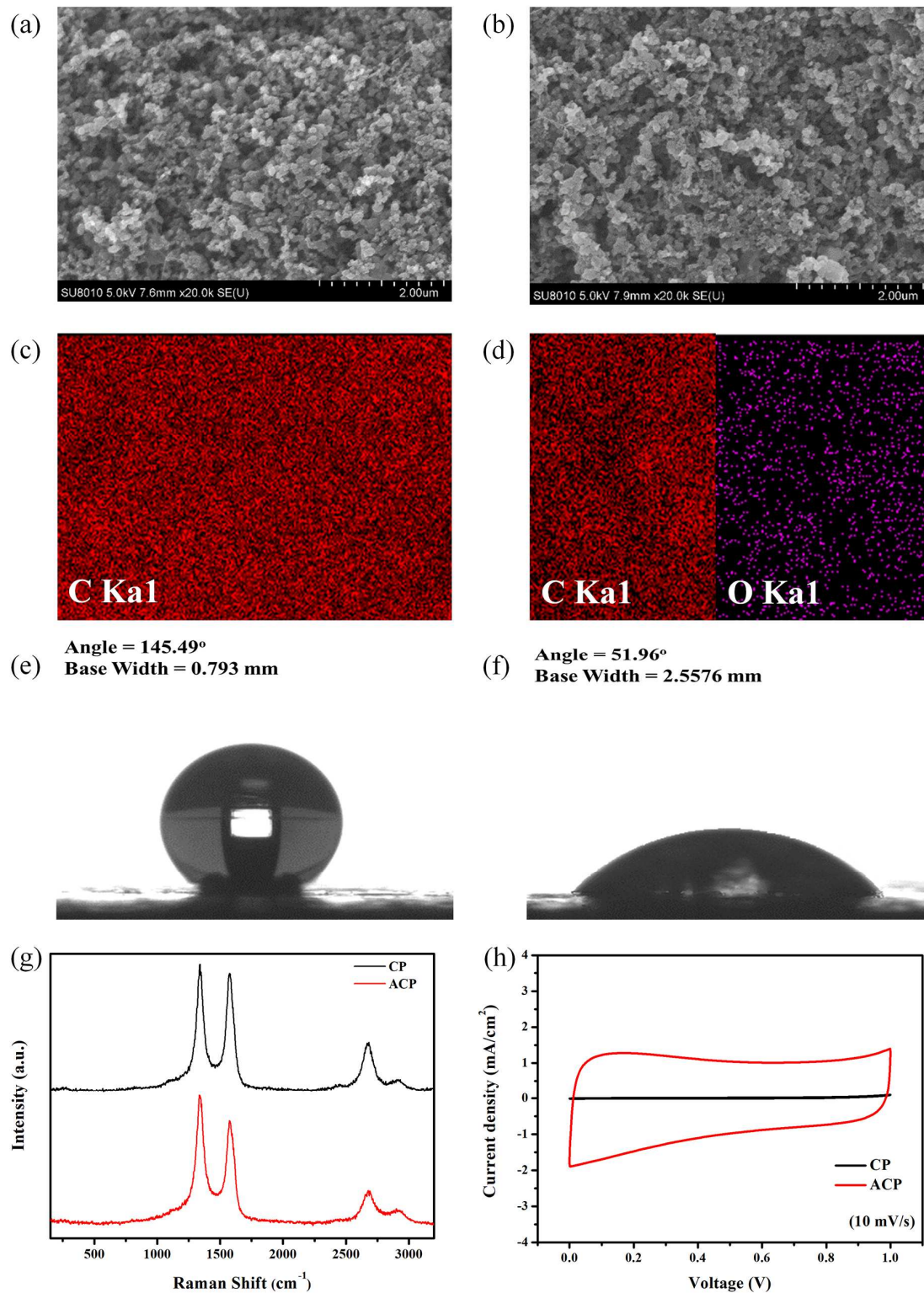
1  
2  
3     3. Characterization of CP and ACP  
4  
5

6     The charge storage of EDLCs is based on the fast arrangements of ions and solvent molecules  
7     and/or adsorption/desorption of ions at the electrode/electrolyte interface within the porous  
8     electrode materials. Thus, porous carbon materials with high surface area are commonly  
9     employed as the electrode materials of EDLCs. However, the hydrated ions are difficult to  
10    diffuse into the porous structure of carbon due to its hydrophobic property which reduces the  
11    accessibility of certain pores and results in the poor charge storage capability. Hence, we  
12    employed the acidic treatment to partially oxidize CPs to form polar functional groups with high  
13    polarity, namely ACPs. The oxygen-containing functional groups cause affinity towards  
14    electrolytes and promote the utilization of CPs for charge storage.  
15  
16

17     The surface morphologies of CP and ACP are characterized by FE-SEM, as shown in Figures  
18     4(a) and 4(b). Both electrodes show a homogeneous porous morphology without any difference,  
19     implying no serious damage on the ACP. Figures 4(c) and 4(d) show the element mapping  
20     results from the energy-dispersive X-Ray spectroscopy. The uniform distribution of carbon  
21     atoms is observable on both materials, however, the ACP exhibits a significant content of  
22     oxygen, ca. 4.86 at%, supporting the formation of oxygen-containing functional groups during  
23     the acidic treatment.  
24  
25

26     Note that the hydrophilicity of CP and ACP can be evaluated by the contact angle analysis and  
27     the results are shown in Figures 4(e) and 4(f). Clearly, CP exhibits a typical hydrophobic  
28     characteristic of carbon, with a contact angle of  $145.49^\circ$  while the contact angle of the CP with  
29     the acidic treatment (i.e., ACP) decreases to  $51.96^\circ$ . Accordingly, the acidic treatment is an  
30     efficient process to improve the hydrophilicity of carbon paper because of the uniform  
31     distribution of oxygen functional groups. The Raman spectra of CP and ACP are shown in  
32  
33

Figure 4(g) where the D, G, and 2D bands are clearly visible. The intensity ratios of D-to-G band ( $I_D/I_G$ ) are 1.07 and 1.23 for CP and ACP, demonstrating the higher structure defects in ACP in comparison with CP. This result is attributable to the damage of carbon caused by acids, probably resulting in the formation of carboxylic groups on ACP.<sup>31</sup> The structure defects and oxygen-containing functional groups on ACP are believed to promote the double-layer charge storage capability because of its hydrophilic surface without considering the additional contributions from the redox reactions and ion adsorption/desorption of the oxygen-containing functional groups. For the intensity ratio of 2D-to-G bands ( $I_{2D}/I_G$ ), CP and ACP distinct similar values of 0.38 and 0.31, respectively, suggesting the superficial damage on the graphitic structure after the acid treatment. The improved charge storage property of CP after the acid treatment can be further confirmed by cyclic voltammetric analysis (see Figure 4(h) where the CV curves were measured at 10 mV s<sup>-1</sup> in a symmetric cell of electrode/WPU-PAAK-K/electrode). From a comparison of these two curves, the ACP/WPU-PAAK-K/ACP cell exhibits tremendous increase in the voltammetric current density, over 700 times higher than that of CP/WPU-PAAK-K/CP. Again, the above results reveal the powerful modification ability of the acid treatment on carbon materials to improve the charge storage capability.<sup>25</sup>



1  
2  
3     **Figure 4.** (a,b) SEM, (c,d) element mapping images and (e,f) contact angle measurement of  
4     (a,c,e) CP and (b,d,f) ACP. (g) Ramon spectra and (h) CV curves measured at 10 mV s<sup>-1</sup> for (1)  
5     CP and (2) ACP.  
6  
7  
8  
9  
10

11     4. Performance comparisons of WPU-PAAK-K and commercial GPEs  
12

13       The use of WPU are enticing owing to its outstanding adhesion property which enables to  
14       bind almost any two materials together. Therefore, WPU-PAAK-K with the polyurethane chains  
15       can improve the adhesion and contact between electrode and GPE in the all-solid-state  
16       supercapacitors. To confirm this idea, the interfaces between ACP and various GPEs (WPU-  
17       PAAK-K, PVA, and PAAK) were carefully checked. The SEM cross-section images of three  
18       GPE/ACP interfaces are shown in Figures 5(a)-5(c). Clearly, the WPU-PAAK-K film closely  
19       adheres to the ACP electrode, attributable to the highly sticky and soft properties of WPU.  
20       However, there is a gap at the PVA/ACP and PAAK/ACP interfaces due to their poor adhesive  
21       and rigid property. These gaps are considered to be the barriers restricting the transport of  
22       electrolytes at interfaces. We also employed the 180°-peeling test to further evaluate the adhesion  
23       characteristics of all GPE films (see Figure 5(d)). The maximum peeling forces of PVA-K,  
24       PAAK-K and WPU-PAAK-K are 30.69, 35.88, and 46.48 N, demonstrating an outstanding  
25       adhesion of WPU-PAAK-K. In addition, the WPU-PAAK-K film shows the better peel  
26       extension than the PVA-K and PAAK-K films since these two films were totally separated at the  
27       peel extension of 0.08 and 1.12 mm<sup>2</sup>. On the contrary, the WPU-PAAK-K film shows an  
28       excellent peel extension property due to the soft property contributed by WPU which makes this  
29       GPE film homogenously sticky onto the testing sample even in a bending situation.  
30  
31  
32  
33  
34  
35  
36  
37  
38  
39  
40  
41  
42  
43  
44  
45  
46  
47  
48  
49  
50  
51  
52  
53  
54  
55  
56  
57  
58  
59  
60

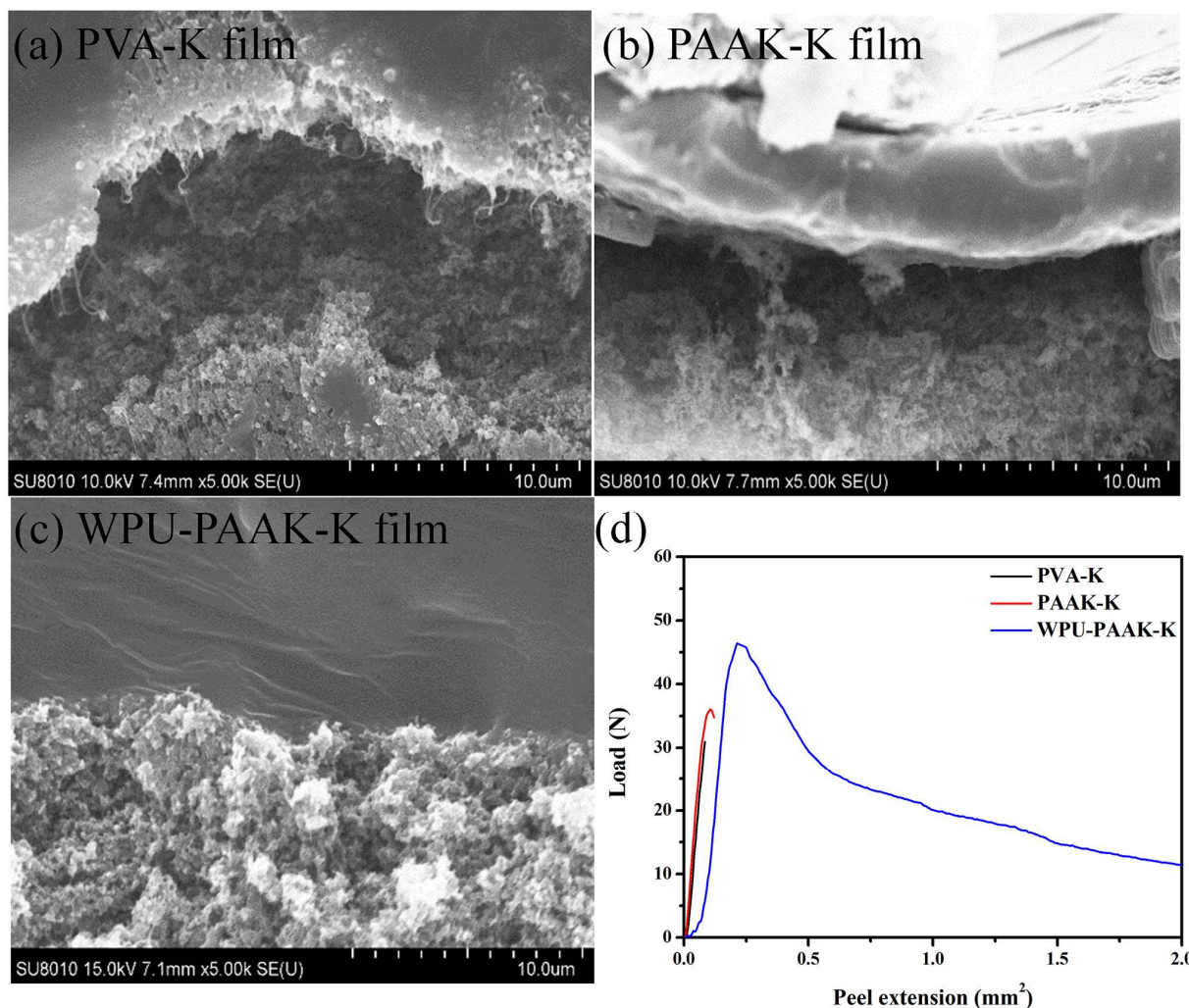


**Figure 5.** SEM cross-section images of the interface between ACP and (a) PVA-K, (b) PAAK-K, and (c) WPU-PAAK-K GPE films. (d) The 180°-peeling test results of three GPE films investigated in this work.

The capacitive characteristics of the above three GPE films with the 200% soaking ratio and the liquid 1 M KOH electrolyte were examined in a coin cell and typical results are shown in Figure 6. From the CV curves measured at a slow scan rate of 10 mV s<sup>-1</sup> in Figure 6(a), all cells (ACP/GPE/ACP) provide typical EDLC responses with quasi-rectangular CV curves, indicating the superb charge storage behavior. The cell containing liquid 1 M KOH electrolyte exhibits the

highest voltammetric current density among these 4 cells due to the easy access of a liquid electrolyte into the pores within the ACP electrode, favoring the electrolyte penetration and utilization of deep pores of ACP. Nevertheless, the voltammetric current density of ACP/WPU-PAAK-K/ACP is similar to that obtained from the liquid electrolyte. Such performance is attributable to the excellent adhesion and contact at the ACP/WPU-PAAK-K interface which facilitates the charge storage process. From these CV curves, the specific capacitance values of ACP in 1 M KOH, PVA-K, PAAK-K, and WPU-PAAK-K electrolytes are 238.2, 166.7, 171.1 and 211.6  $\text{mF cm}^{-2}$ , respectively. In Figure 6(b), the ACP/WPU-PAAK-K/ACP cell still maintains the quasi-rectangular CV curve at a high scan rate of 100  $\text{mV s}^{-1}$ , indicating an excellent EDLC behavior. For the commercial GPE films of PVA-K and PAAK-K, the gaps at the ACP/GPE interface should limit the diffusion of electrolyte ions, probably resulting in a high contact resistance. The cell using liquid 1 M KOH reports a relatively high equivalent series resistance (ESR), implied by a distorted CV curve, probably resulting from the usage of a separator preventing the short circuit between two electrodes. From a comparison of all CV curves in Figure 6(b), the CV distortion at a high scan rate is very serious for the devices using PVA-K and PAAK-K GPEs, reasonably attributed to the significant contact resistance at the ACP/GPE interface. The area-based specific capacitance values of ACP at 100  $\text{mV s}^{-1}$  are 166.1, 98.2, 113.6 and 156.3  $\text{mF cm}^{-2}$  in 1 M KOH, PVA-K, PAAK-K, and WPU-PAAK-K, respectively. The ACP/KOH/ACP cell exhibits the highest specific capacitance among all cells whereas the ACP/WPU-PAAK-K/ACP device shows better EDLC responses from the quasi-rectangular CV curve, reasonably due to the improved electrolyte/electrode interface.

The EIS spectra were used to further investigate the impedance sources of the above cells and typical Nyquist plots of these four devices are shown in Figure 6(c). The EIS data can be divided

1  
2  
3 into three sections. In the high-frequency region, the real part resistance at the high-frequency  
4 end is associated with the ESR mainly contributed by the electrolyte resistance. The cell with 1  
5 M KOH electrolyte solution demonstrates the lowest resistance due to the high ionic  
6 conductivity above  $10^{-1}$  S cm<sup>-1</sup>. The GPE films in the supercapacitors provide the flexibility but  
7 restrict the transport of electrolytes, leading to the reduced ionic conductivity. In the middle-  
8 frequency region, the semicircle may be contributed by two mechanisms: charge-transfer  
9 impedance from the redox functional groups on ACPs and contact impedance at the porous ACP  
10 electrode/electrolyte interface. Note that the charge transfer resistances in all devices should be  
11 very similar because all cells employ the same type of ACPs and KOH is the main ion-  
12 conductive medium. Accordingly, the variation in the semicircle impedance is believed to result  
13 from the contact resistance at the porous ACP electrode/electrolyte interface. Interestingly, the  
14 ACP/WPU-PAAK-K/ACP cell shows the lowest real-part impedance in the semicircle (0.44 Ω)  
15 among all devices, revealing the unique binder function of this GPE which improves the contact  
16 at the interface between electrode and electrolyte. The cell using 1 M KOH with a separator and  
17 those with PVA-K and PAAK-K GPEs result in a relatively high real-part impedance in  
18 semicircles (2.29, 6.65 and 5.14 Ω, respectively). Finally, the almost vertical lines in the low-  
19 frequency region reveal the typical capacitor behavior for all devices.  
20  
21

22  
23  
24 Figure 6(d) shows the typical charge-discharge curves of the above four devices at a high current  
25 density in order to clearly observe the *iR* drops. Manifestly, the cell voltages on all curves are  
26 generally linear in the charge and discharge periods, revealing the typical supercapacitor  
27 responses of all devices investigated here. However, the order of electrolytes in these  
28 supercapacitors with respect to increasing the *iR* drop is: WPU-PAAK-K (0.05 V) < 1 M KOH  
29 (0.09 V) < PAAK-K (0.15 V) < PVA-K (0.23 V). Again, the ACP/WPU-PAAK-K/ACP cell  
30  
31  
32  
33  
34  
35  
36  
37  
38  
39  
40  
41  
42

with the smallest  $iR$  drop reveals the excellent binder function of the WPU-PAAK-K film on improving the contact at the electrode/electrolyte interface.

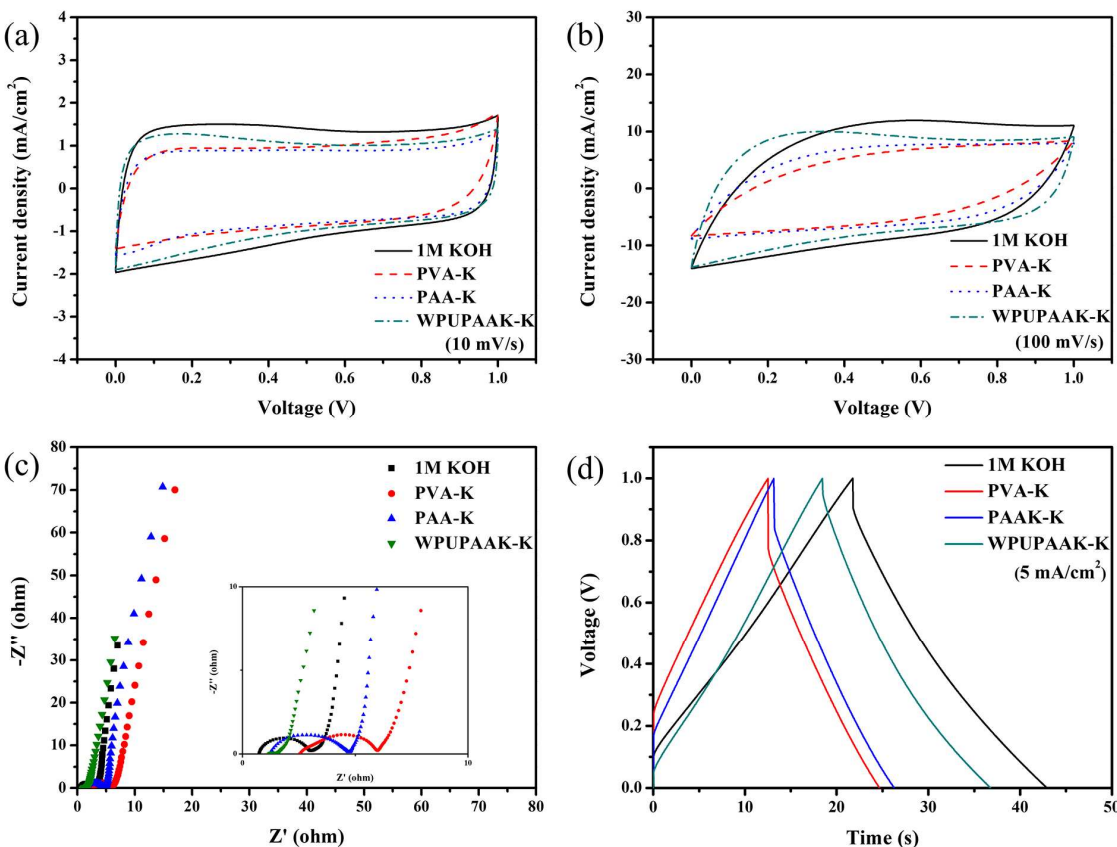


**Figure 6.** (a,b) CV curves measured at (a) 10 and (b) 100  $\text{mV s}^{-1}$ , (c) EIS spectra from 10 kHz to 10 mHz, and (d) charge-discharge curves at 5  $\text{mA cm}^{-2}$  for the cells using (1) 1 M KOH, (2) PVA-K, (3) PAAK-K, and (4) WPU-PAAK-K as electrolytes.

## 5. Characterization of an un-packed ACP/WPU-PAAK-K/ACP cell

Recently, the safety concerns in energy storage devices are rising because of the increasing demands on wearable devices. The leakage of liquid electrolytes will lead to dangerous issues and the volatile organics will cause expansion of compact systems. Here, an all-solid-state ACP/WPU-PAAK-K/ACP EDLC without any package is designed to circumvent these issues.

Note that the WPU-PAAK polymer as the aqueous electrolyte absorbent can avoid the leakage of electrolyte and enhance the electrolyte retention because of its network structure. In addition, due to the strong adhesion characteristics of this WPU-PAAK-K film, the device without any package is not peeled off under various kinds of storage (e.g., vertical or 45° placement).

The capacitive performances of this un-packed ACP/WPU-PAAK-K/ACP device are shown in Figure 7. Figure 7(a) shows that the CV curves of this EDLC are of the quasi-rectangular shape as the scan rate is varied from 10 to 100 mV s<sup>-1</sup>, revealing the good capacitive performance. The charge-discharge curves of this device are shown in Figure 7(b). All curves show nearly triangular shapes at 1-10 mA cm<sup>-2</sup>, indicating the ideal capacitive performance although a minor distortion is found at cell voltage > 0.9 V at a low current density. The specific capacitance of this device ranges from 94.6 to 56.7 mF cm<sup>-2</sup> with increasing the current density from 1 to 10 mA cm<sup>-2</sup>. This all-solid-state EDLC shows excellent cycling stability in the galvanic charge-discharge test at 1 mA cm<sup>-2</sup> (see Figure 7(c) where the cell capacitance retention remains 94 % after the 10000-cycle test). In addition, this device also shows fairly high power density and energy density in the Ragone plot from Figure 7(d). The energy density can reach 13.14 and 7.88 μWh cm<sup>-2</sup> at a power density of 0.5 and 5 mW cm<sup>-2</sup> and a current density of 1 and 10 mA cm<sup>-2</sup>, respectively. These values are much higher than the results reported in some recent articles, such as rGO-PEDOT:PSS (4.55 μWh cm<sup>-2</sup> at 1.5 mW cm<sup>-2</sup>)<sup>32</sup>, 3D-graphene/graphite (1.24 μWh cm<sup>-2</sup> at 0.024 mW cm<sup>-2</sup>)<sup>33</sup>, polypyrrole arrays (4 μWh cm<sup>-2</sup> at 0.185 mW cm<sup>-2</sup>)<sup>34</sup> and MWCNT/V<sub>2</sub>O<sub>5</sub> (3.31 μWh cm<sup>-2</sup> at 0.387 mW cm<sup>-2</sup>)<sup>35</sup>.

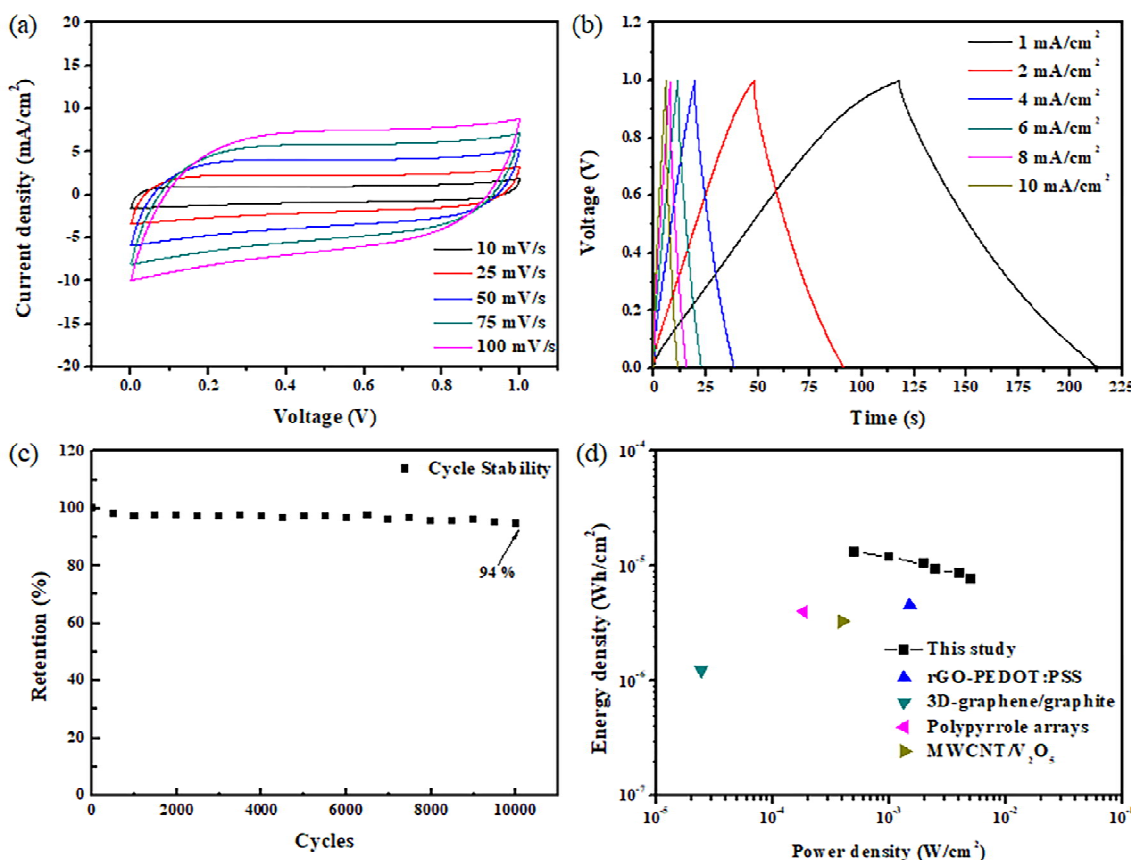


**Figure 7.** (a) CV and (b) charge-discharge curves and (c) capacitance retention of a non-packaged ACP/WPU-PAAK-K/ACP EDLC, and (d) the corresponding Ragone plot with comparisons of the literature data.<sup>32-35</sup>

To demonstrate the flexibility of the above EDLC, its capacitive behavior measured at various bending situations is shown in Figure 8. Figure 8(a) shows the photos of single electrode and prove an outstanding flexibility under the bending situation. The assembled ACP/WPU-PAAK-K/ACP device without any package is reported in Figure 8(b) which shows the excellent layer-by-layer stacking without separation even under the bending situation. The CV curves measured at 50 mV s<sup>-1</sup> and the charge-discharge curves at 2 mA cm<sup>-2</sup> under different bending angles are shown in Figures 8(c) and 8(d). All these results confirm the excellent capacitive behavior of this

all solid-state EDLC without significant ESR from the slightly distorted CV and CP curves. The discharge specific capacitance of this EDLC reaches 81.6, 80.6, 80.2, 79.8 and 75.1 mF cm<sup>-2</sup> at 2 mA cm<sup>-2</sup> when the bending angle is varied from 0 to 180°. This result reveals over 90 % specific capacitance retention at a bending angle of 180°, suggesting the perfect flexibility of this non-packed EDLC which is never reported before. The above-mentioned excellent flexibility of this EDLC is reasonably attributed to the unique bi-functions of our WPU-PAAK-K GPE working perfectly as an ionic conductor and a binder.

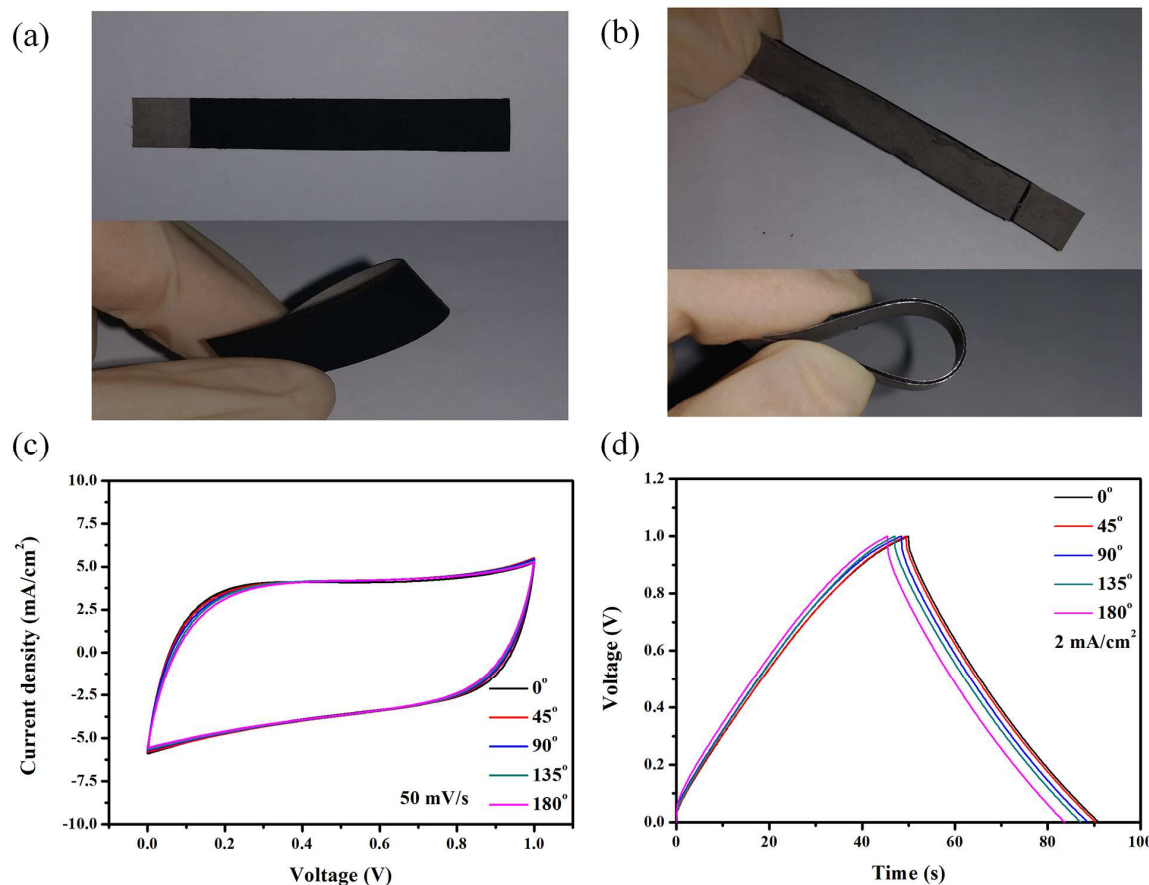


**Figure 8.** (a, b) The photos of (a) a flexible electrode and (b) the device; (c) CV and (d) CP curves of a non-packaged ACP/WPU-PAAK-K/ACP EDLC at various bending angles.

## CONCLUSION

The cross-linked network structure of the newly designed WPU-PAA polymer has been successfully synthesized from WPU and PAA, which exhibits excellent adhesive and electrolyte-uptake properties from WPU and PAA, respectively. The WPU-PAAK-K GPE film with a 200% soaking ratio shows a high ionic conductivity of  $9.6 \times 10^{-2}$  S cm<sup>-1</sup>. The ACP/WPU-PAAK-K/ACP device in the coin cell test displays a distinguished specific capacitance of 211.6 mF cm<sup>-2</sup> at 10 mV s<sup>-1</sup> for ACPs and a low contact resistance of 0.44 Ω in the middle-frequency semicircle from the EIS study. This work also first time demonstrates an all-solid-state, flexible, non-packed supercapacitor consisting of ACP/WPU-PAAK-K/ACP. The EDLC shows a fairly high specific capacitance of 94.6 mF cm<sup>-2</sup> at a current density of 1 mA cm<sup>-2</sup>. Its energy density reaches 13.14 and 7.88 μWh cm<sup>-2</sup> at a power density of 0.5 and 5 mW cm<sup>-2</sup> and a current density of 1 and 10 mA cm<sup>-2</sup>, respectively. In the bending test, the device exhibits an outstanding flexibility and over 90% capacitance retention at bending angle of 180°.

## AUTHOR INFORMATION

Corresponding Author

ccma@che.nthu.edu.tw; cchu@che.nthu.edu.tw.

Present Addresses

Department of Chemical Engineering National Tsing-Hua University Hsin-Chu 30013, Taiwan

Author Contributions

The manuscript was written through contributions of all authors. All authors have given approval to the final version of the manuscript. ‡These authors contributed equally.

1  
2  
3       **ACKNOWLEDGMENT**  
4  
5  
6  
7  
8  
9  
10  
11  
12  
13  
14  
15  
16  
17  
18  
19  
20  
21  
22  
23  
24  
25  
26  
27  
28  
29  
30  
31  
32  
33  
34  
35  
36  
37  
38  
39  
40  
41  
42  
43  
44  
45  
46  
47  
48  
49  
50  
51  
52  
53  
54  
55  
56  
57  
58  
59  
60

The financial support of this research, by the Ministry of Science and Technology of the Taiwan, under contract no. MOST 105-2221-E-007-127-MY3, 106-2221-E-007-089-MY3, and the boost program of the Lower Carbon Energy Research Center in NTHU, are gratefully acknowledged.

1  
2  
3 REFERENCES  
4  
5

- 6 (1) Yang, Z.; Zhang, J.; Kintner-Meyer, M. C.; Lu, X.; Choi, D.; Lemmon, J. P.; Liu, J.  
7 Electrochemical Energy Storage for Green Grid. *Chem Rev* **2011**, *111* (5), 3577-613, DOI:  
8 10.1021/cr100290v.
- 9 (2) R. Koitz, M. C. Principles and Applications of Electrochemical Capacitors. *Electrochimica  
10 Acta* **2000**, *45*, 2483-2498.
- 11 (3) Bai, N.; Xu, Z.; Tian, Y.; Gai, L.; Jiang, H.; Marcus, K.; Liang, K. Tailorable Polypyrrole  
12 Nanofilms with Exceptional Electrochemical Performance for All-Solid-State Flexible  
13 Supercapacitors. *Electrochimica Acta* **2017**, *249*, 360-368, DOI: 10.1016/j.electacta.2017.08.034.
- 14 (4) Christinelli, W. A.; Gonçalves, R.; Pereira, E. C. A New Generation of Electrochemical  
15 Supercapacitors Based on Layer-by-Layer Polymer Films. *Journal of Power Sources* **2016**, *303*,  
16 73-80, DOI: 10.1016/j.jpowsour.2015.10.077.
- 17 (5) Cai, G.; Darmawan, P.; Cui, M.; Wang, J.; Chen, J.; Magdassi, S.; Lee, P. S. Highly Stable  
18 Transparent Conductive Silver Grid/Pedot:Pss Electrodes for Integrated Bifunctional Flexible  
19 Supercapacitors. *Advanced Energy Materials* **2016**, *6* (4), 1501882, DOI:  
20 10.1002/aenm.201501882.
- 21 (6) Sumboja, A.; Foo, C. Y.; Wang, X.; Lee, P. S. Large Areal Mass, Flexible and Free-Standing  
22 Reduced Graphene Oxide/Manganese Dioxide Paper for Asymmetric Supercapacitor Device.  
23 *Adv Mater* **2013**, *25* (20), 2809-15, DOI: 10.1002/adma.201205064.
- 24 (7) Yan, C.; Wang, J.; Kang, W.; Cui, M.; Wang, X.; Foo, C. Y.; Chee, K. J.; Lee, P. S. Highly  
25 Stretchable Piezoresistive Graphene-Nanocellulose Nanopaper for Strain Sensors. *Adv Mater*  
26 **2014**, *26* (13), 2022-7, DOI: 10.1002/adma.201304742.
- 27 (8) Ren, J.; Bai, W.; Guan, G.; Zhang, Y.; Peng, H. Flexible and Weaveable Capacitor Wire

1  
2  
3 Based on a Carbon Nanocomposite Fiber. *Adv Mater* **2013**, *25* (41), 5965-70, DOI:  
4  
5 10.1002/adma.201302498.  
6  
7

8 (9) Meng, Y.; Zhao, Y.; Hu, C.; Cheng, H.; Hu, Y.; Zhang, Z.; Shi, G.; Qu, L. All-Graphene Core-  
9 Sheath Microfibers for All-Solid-State, Stretchable Fibriform Supercapacitors and Wearable  
10 Electronic Textiles. *Adv Mater* **2013**, *25* (16), 2326-31, DOI: 10.1002/adma.201300132.  
11  
12

13 (10) Ramadoss, A.; Saravanakumar, B.; Kim, S. J. Thermally Reduced Graphene Oxide-Coated  
14 Fabrics for Flexible Supercapacitors and Self-Powered Systems. *Nano Energy* **2015**, *15*, 587-  
15 597, DOI: 10.1016/j.nanoen.2015.05.009.  
16  
17

18 (11) Xu, J.; Wang, D.; Yuan, Y.; Wei, W.; Duan, L.; Wang, L.; Bao, H.; Xu, W. Polypyrrole/Reduced Graphene Oxide Coated Fabric Electrodes for Supercapacitor Application.  
19  
20 *Organic Electronics* **2015**, *24*, 153-159, DOI: 10.1016/j.orgel.2015.05.037.  
21  
22

23 (12) Xu, J.; Wang, D.; Fan, L.; Yuan, Y.; Wei, W.; Liu, R.; Gu, S.; Xu, W. Fabric Electrodes  
24 Coated with Polypyrrole Nanorods for Flexible Supercapacitor Application Prepared Via a  
25 Reactive Self-Degraded Template. *Organic Electronics* **2015**, *26*, 292-299, DOI:  
26 10.1016/j.orgel.2015.07.054.  
27  
28

29 (13) Xie, Y.; Liu, Y.; Zhao, Y.; Tsang, Y. H.; Lau, S. P.; Huang, H.; Chai, Y. Stretchable All-Solid-  
30 State Supercapacitor with Wavy Shaped Polyaniline/Graphene Electrode. *J. Mater. Chem. A*  
31  
32 **2014**, *2* (24), 9142-9149, DOI: 10.1039/c4ta00734d.  
33  
34

35 (14) Li, X.; Zhao, T.; Chen, Q.; Li, P.; Wang, K.; Zhong, M.; Wei, J.; Wu, D.; Wei, B.; Zhu, H. Flexible All Solid-State Supercapacitors Based on Chemical Vapor Deposition Derived Graphene  
36 Fibers. *Phys Chem Chem Phys* **2013**, *15* (41), 17752-7, DOI: 10.1039/c3cp52908h.  
37  
38

39 (15) Zhi, J.; Yang, C.; Lin, T.; Cui, H.; Wang, Z.; Zhang, H.; Huang, F. Flexible All Solid State  
40 Supercapacitor with High Energy Density Employing Black Titania Nanoparticles as a  
41  
42

1  
2  
3 Conductive Agent. *Nanoscale* **2016**, *8* (7), 4054-62, DOI: 10.1039/c5nr08136j.  
4  
5

6 (16) Vijayakumar, V.; Anothumakkool, B.; Torris A. T, A.; Nair, S. B.; Badiger, M. V.; Kurungot,  
7 S. An All-Solid-State-Supercapacitor Possessing a Non-Aqueous Gel Polymer Electrolyte  
8 Prepared Using a Uv-Assisted in Situ Polymerization Strategy. *J. Mater. Chem. A* **2017**, *5* (18),  
9 8461-8476, DOI: 10.1039/c7ta01514c.  
10  
11

12 (17) Li, J.; Qiao, J.; Lian, K. Investigation of Polyacrylamide Based Hydroxide Ion-Conducting  
13 Electrolyte and Its Application in All-Solid Electrochemical Capacitors. *Sustainable Energy &*  
14 *Fuels* **2017**, *1* (7), 1580-1587, DOI: 10.1039/c7se00266a.  
15  
16

17 (18) Palaniappan, R.; Botte, G. G. Efficacy of Potassium Poly(Acrylate) Gel Electrolyte as a  
18 Substitute to Aqueous Electrolytes for Alkaline Ammonia Electrolysis. *Electrochimica Acta*  
19 **2013**, *88*, 772-781, DOI: 10.1016/j.electacta.2012.10.023.  
20  
21

22 (19) Gao, H.; Lian, K. Proton-Conducting Polymer Electrolytes and Their Applications in Solid  
23 Supercapacitors: A Review. *RSC Adv.* **2014**, *4* (62), 33091-33113, DOI: 10.1039/c4ra05151c.  
24  
25

26 (20) Shinji Nohara, H. W., Naoki Furukawa, Hiroshi Inoue, Masayuki Morita, Chiaki Iwakura.  
27 Electrochemical Characterization of New Electric Double Layer Capacitor with Polymer  
28 Hydrogel Electrolyte. *Electrochimica Acta* **2003**, *48*, 749-753.  
29  
30

31 (21) Ten-Chin Wena, Y.-J. W., Tsung-Tien Chenga, Chien-Hsin Yangb. The Effect of Dmpa Units  
32 on Ionic Conductivity of Peg-Dmpa-Ipdi Waterborne Polyurethane as Single-Ion Electrolytes.  
33 *polymer* **1999**, *40*, 3979-3988.  
34  
35

36 (22) Xing, Y.; Wu, Y.; Wang, H.; Yang, G.; Li, W.; Xu, L.; Jiang, X. Preparation of Hybrid  
37 Polymer Based on Polyurethane Lithium Salt and Polyvinylidene Fluoride as Electrolyte for  
38 Lithium-Ion Batteries. *Electrochimica Acta* **2014**, *136*, 513-520, DOI:  
39 10.1016/j.electacta.2014.05.122.  
40  
41

- (23) Yu, R.; Bao, J.-J.; Chen, T.-T.; Zou, B.-K.; Wen, Z.-Y.; Guo, X.-X.; Chen, C.-H. Solid Polymer Electrolyte Based on Thermoplastic Polyurethane and Its Application in All-Solid-State Lithium Ion Batteries. *Solid State Ionics* **2017**, *309*, 15-21, DOI: 10.1016/j.ssi.2017.06.013.
- (24) Xiao, Y.; Jiang, L.; Liu, Z.; Yuan, Y.; Yan, P.; Zhou, C.; Lei, J. Effect of Phase Separation on the Crystallization of Soft Segments of Green Waterborne Polyurethanes. *Polymer Testing* **2017**, *60*, 160-165, DOI: 10.1016/j.polymertesting.2017.03.029.
- (25) Hu, C.-C.; Su, J.-H.; Wen, T.-C. Modification of Multi-Walled Carbon Nanotubes for Electric Double-Layer Capacitors: Tube Opening and Surface Functionalization. *Journal of Physics and Chemistry of Solids* **2007**, *68* (12), 2353-2362, DOI: 10.1016/j.jpcs.2007.07.002.
- (26) S.R. Leadley, J. F. W. The Use of Xps to Examine the Interaction of Poly(Acrylic Acid) with Oxidised Metal Substrates. *Journal of electron spectroscopy* **1997**, *85*, 107-121.
- (27) Wu, G.; An, J.; Sun, D.; Tang, X.; Xiang, Y.; Yang, J. Robust Microcapsules with Polyurea/Silica Hybrid Shell for One-Part Self-Healing Anticorrosion Coatings. *J. Mater. Chem. A* **2014**, *2* (30), 11614-11620, DOI: 10.1039/c4ta01312c.
- (28) G. Beamson, D. B. *High Resolution Xps of Organic Polymers - the Scienta Esca300 Database* Wiley Interscience, 1992.
- (29) Killis, A.; LeNest, J.-F.; Gandini, A.; Cheradame, H.; Cohen-Addad, J.-P. Correlation between Ionic Conductivity and <sup>7</sup>Li-Nmr of Polyether-Polyurethane Networks Containing Lithium Perchlorate. *Polymer Bulletin* **1982**, *6* (7), 351-358.
- (30) Pan, J.; Chen, C.; Li, Y.; Wang, L.; Tan, L.; Li, G.; Tang, X.; Xiao, L.; Lu, J.; Zhuang, L. Constructing Ionic Highway in Alkaline Polymer Electrolytes. *Energy & Environmental Science* **2014**, *7* (1), 354-360.
- (31) Bai, H.; Li, C.; Shi, G. Functional Composite Materials Based on Chemically Converted

1  
2  
3 Graphene. *Advanced Materials* **2011**, *23* (9), 1089-1115.  
4  
5

6 (32) Li, B.; Cheng, J.; Wang, Z.; Li, Y.; Ni, W.; Wang, B. Highly-Wrinkled Reduced Graphene  
7 Oxide-Conductive Polymer Fibers for Flexible Fiber-Shaped and Interdigital-Designed  
8 Supercapacitors. *Journal of Power Sources* **2018**, *376*, 117-124, DOI:  
9  
10 10.1016/j.jpowsour.2017.11.076.  
11  
12

13 (33) Ramadoss, A.; Yoon, K.-Y.; Kwak, M.-J.; Kim, S.-I.; Ryu, S.-T.; Jang, J.-H. Fully Flexible,  
14 Lightweight, High Performance All-Solid-State Supercapacitor Based on 3-Dimensional-  
15 Graphene/Graphite-Paper. *Journal of Power Sources* **2017**, *337*, 159-165, DOI:  
16  
17 10.1016/j.jpowsour.2016.10.091.  
18  
19

20 (34) Li, L.; Fu, C.; Lou, Z.; Chen, S.; Han, W.; Jiang, K.; Chen, D.; Shen, G. Flexible Planar  
21 Concentric Circular Micro-Supercapacitor Arrays for Wearable Gas Sensing Application. *Nano*  
22  
23 *Energy* **2017**, *41*, 261-268, DOI: 10.1016/j.nanoen.2017.08.060.  
24  
25

26 (35) Kim, D.; Keum, K.; Lee, G.; Kim, D.; Lee, S.-S.; Ha, J. S. Flexible, Water-Proof, Wire-Type  
27 Supercapacitors Integrated with Wire-Type Uv/No 2 Sensors on Textiles. *Nano Energy* **2017**, *35*,  
28 199-206, DOI: 10.1016/j.nanoen.2017.03.044.  
29  
30  
31  
32  
33  
34  
35  
36  
37  
38  
39  
40  
41  
42  
43  
44  
45  
46  
47  
48  
49  
50  
51  
52  
53  
54  
55  
56  
57  
58  
59  
60

## TABLE OF CONTENTS

